

# **Adaptive Reshaping of Objects in (Multiparameter) Hilbert Space for Enhanced Detection and Classification: An Application of Receiver Operating Curve (ROC) Statistics to Laser-Based Mass Spectroscopy**

Dmitri Romanov<sup>1</sup>, Dennis Healy<sup>2</sup>, John Brady<sup>1</sup>, Robert J. Levis<sup>1</sup>

<sup>1</sup> Center for Advanced Photonics Research, Temple University, Philadelphia, PA 19122

<sup>2</sup> Department of Mathematics, University of Maryland, College Park, MD 20742

## **Abstract.**

We propose a new approach to classical detection problem of discrimination of a true signal of interest from an interferent signal. We show that the detection performance, as quantified by the receiver operating curve (ROC), can be substantially improved when the signal is represented by a multi-component data set that is actively manipulated by means of a shaped laser probe pulse. In this case, the signal sought (agent) and the interfering signal (interferent) are visualized by vectors in a multi-dimensional detection space. Separation of these vectors can be achieved by adaptive modification of a probing laser pulse to actively manipulate the Hamiltonian of the agent and interferent. We demonstrate one implementation of the concept of adaptive rotation of signal vectors to chemical agent detection by means of strong-field time-of-flight mass-spectrometry.

## **1. Introduction**

A classical detection problem is the binary hypothesis testing problem: that is to decide whether measured data reveal the presence of true signal or whether these data just represent the presence of noise/interfering signal. A typical example is a radar detection system that probes surroundings with a microwave beam and analyzes the echo waves to determine whether a suspicious object is present and furthermore, whether this object is, for instance, a tank or a school bus. Thus, the outcome of a typical detection process is the decision as to whether the target signal is present. To produce a decision, the detection system typically comprises several layers of signal processing: (i) physical layer, where the raw sensing data are collected; (ii) preprocessing layer, where the data are sifted and rearranged to facilitate extraction of meaningful features; (iii) exploitation layer where the extracted features are analyzed and the final decision is made. Traditionally, collection of as much raw information on the physical layer was assumed to be beneficial, thus relegating the task of organizing this information (properly digitized) to the processing layer. However, indefinitely increasing the amount of sensing information *per se* does not improve the overall system performance due to “the curse of dimensionality” that forces the system to use almost all its resources to represent

irrelevant portions of the search space [1, 2]. This is especially so in real-time settings. The answer to this conundrum was the concept of integrating sensing and processing (ISP) [3]. Integrated sensing and processing emphasizes extending the information filtering to the physical layer, operating in a feedback mode with the processing layer (Fig. 1a). The physical layer often encompasses probe and detection subsystems. In this paper, we make the further natural step: we suggest proactive detection approach that includes adaptive manipulation of the physical layer. This manipulation channels the probe-target interaction to produce most distinguishable signals in some chosen low-dimensional representation. In this paper, a probe laser pulse interacting with a target sample. Thus, in this example we are adaptively manipulating the probe-target interaction by manipulating the characteristics of the probe laser pulse. The important point is that a portion of the distributed decision-making process is transferred to active manipulation of the Hamiltonian of the system itself. As a general rule, control of the time-dependent features of the probing beam is possible and simple to implement, while similar manipulation of the detection system is intractable.

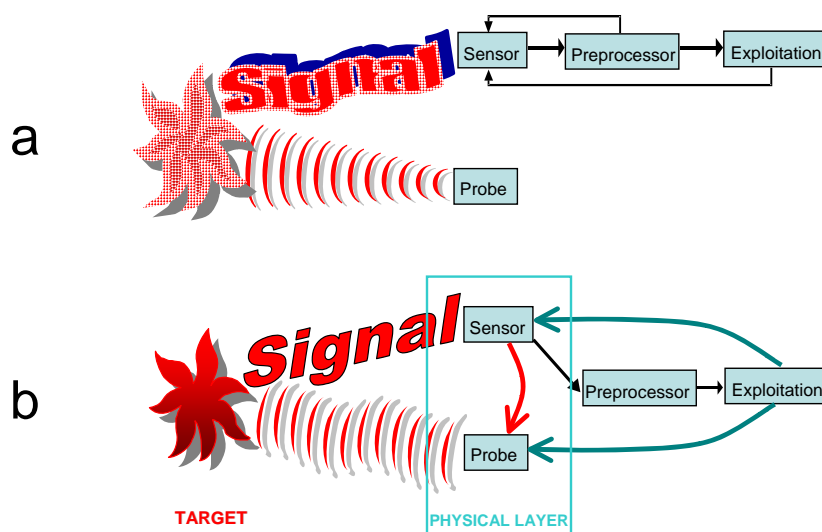


**Figure 1.** **a**, integrated sensing and processing where the initial sensor measurements are processed in the preprocessor. Both preprocessor and exploitation level operate in feedback mode suggesting adjustments to the sensor. **b**, the proposed modification where the physical layer includes adaptive feedback loop controlling the probe to optimize the measured signal.

The success of adaptive probe manipulation (or active Hamiltonian manipulation) depends on the ability to arbitrarily explore vast amounts of information in the search space on a rapid timescale and to change at will the dimensionality of this search space. This places certain functional requirements on the probe and detection system. As an example of an important and instructive implementation, we consider here laser-based time-of-flight (TOF) mass spectrometry as a multiparameter method of chemical agent

detection. Traditionally, most analytical techniques involve scalar measurements. They employ two kinds of detection methods: (i), measurement of a single characteristic quantity of a molecule is made (such as acidity, polarizability, permanent dipole, etc.) and the system is classified by the value of this quantity; (ii), a specific probing signal is applied, and a positive/negative response of the system is measured (as in laser induced fluorescence, for example). Time-of-flight mass spectrometry measures a fragmentation pattern (the mass spectrum) that represents an individual chemical agent as a particular fingerprint of fragment ion signals. The given mass spectral pattern represents a collection of scalar measurements that recently has become an area for active manipulation making for effective confluence of the two detection approaches [4].

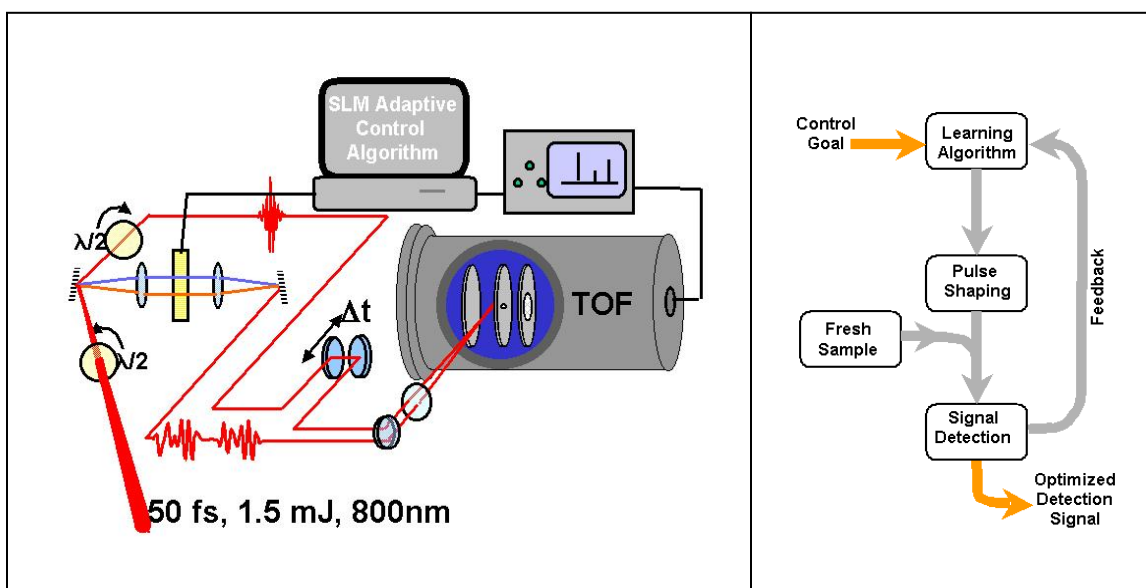


**Fig. 2.** A schematic of a control loop for mass spectral identification of molecular species. The control pulse is optimized by adaptive learning. The computer monitors the outcome of the intense laser-molecule interaction via time-of-flight mass spectrometry, evaluates the outcome via a fitness function, and creates new pulse shapes based on fitness. The process iterates until the desired outcome is obtained.

In the recent times, time-of-flight mass spectroscopy combined with laser-induced dissociative ionization has evolved into an important method of quantitative chemical analysis. The method allows measurement of molecular fragments following the fragmentation of a molecule induced by an intense laser pulse (see Fig. 2). In this type of experiment, the measured mass spectrum bears imprints of the molecule under investigation and of the laser pulse that produces the dissociation. Other types of mass spectrometry (electron impact, chemical ionization, electrospray ionization) focus on signal processing and pattern analysis in similar applications to pick out signature features. However, a quantum leap in TOF analysis was achieved when it became possible to replace conventional ionization sources with tailored laser pulses that have an enormous capacity for varying the fragmentation distribution [4]. This is related to the realization that closed-loop methods can be used in laser-based experiments to search a

large space of potential laser pulse shapes [5]. This particular mass-spectral detection method has an advantage in that any molecule has some probability to fragment, depending on the shape of the intense laser pulse, producing a distribution of ions, each of which contributes to determining the identity of the molecule under analysis.

Strong-field laser mass spectrometry utilizes the highly nonlinear interaction of an intense laser field (a short laser pulse of  $\sim 50$  fs duration and  $\sim 10^{14}$  W/cm<sup>2</sup> intensity) with a molecule. In this case, a laser pulse with wavelength  $800 \pm 5$  nm is sufficient to ionize virtually any gas phase molecule to provide both intact parent ion and/or various ionization fragments. This ionization method is ideally linked to time-of-flight mass spectrometry for rapid structural identification because of the pulsed nature of the excitation process. The combination provides a detector system capable of recording all ions for all species in a mixture in less than one thousandth of a second. Investigations have revealed that the ionized fragment distribution for a given molecule can be easily altered by manipulating either the pulse duration or the intensity of the laser. This capability is being developed to control chemical reactivity in several research laboratories at the present time [6-9]. Recent experiments on high-field control [10, 11] also demonstrated that strong fields can create and manipulate a rich variety of final product state distributions for subsequent manipulation (see Fig. 3).

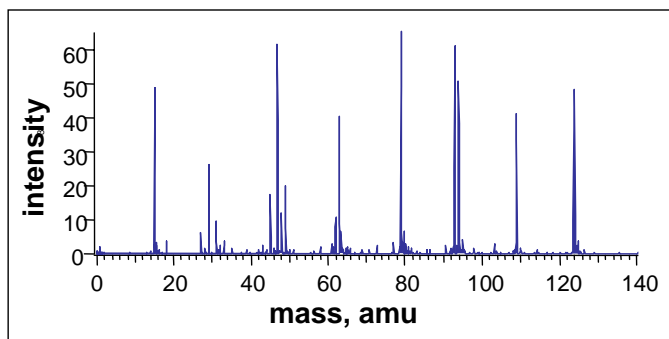


**Figure 3.** A typical mass-spectrum of a complex molecule (dimethylmethylphosphonate subjected to a transform-limited pulse of  $10^{13}$  W·cm<sup>-2</sup> intensity and 60 fs duration), which displays a variety of dissociation fragments.

The enabling technology for the intended manipulation of the mass-spectroscopic data vectors is control of the laser pulse shape, to manipulate, in turn, the mass spectral fragmentation distribution. This involves, first of all, the production of stable, intense ultrashort laser pulses [12] with a high repetition rate. Typically, the optical system is based on the Ti:sapphire laser having a bandwidth between 750 and 950 nm and pulse duration as short as 6 fs. After regenerative amplification, laser pulses are produced on the order of several mJ with duration as short as 40 fs. Then, these pulses are controllably shaped using liquid crystal, spatial light-modulation techniques [8, 13-15]. The laser beam is dispersed using an optical grating and collimated using a lens as shown in Fig. 4. The phase or amplitude (or both) of the spatially separated individual frequency

components of the laser beam are modulated using a spatial mask located in the Fourier plane of the zero length stretcher. The modulated beam is then focused onto a second grating to create the shaped laser pulse that will interact with the molecule. In this way, one can create a vast array of tailored pulse shapes to interact with the system of interest. The tailored pulses can be amplified in energy to access the strong field regime, where the electric field of the light pulse is as strong as the fields binding electrons within a molecule. This regime opens up a number of mechanisms for energy coupling [16] and makes possible various scenarios of molecular fragmentation [4]. The fragmentation pattern (the probability to produce a given ionized fragment of the initial molecule) is thus uniquely determined by the pulse shape (the maximum amplitude, the amplitude envelope, and the phase envelope).

We show in this paper that adaptive strong-field TOF mass-spectrometry allows proactive detection to be easily achieved and that adaptive changing of the nonlinear interaction between the tailored strong-field laser pulse and the target molecule considerably increases the discrimination between chemical agents of interest and mimicking interferents. Upon developing a proper protocol, the proposed detection method will be able to project the molecule in question onto the set of library features at the stage of interaction, eliminating the costly necessity to manipulate the sensor read-out space to achieve a feature-clarifying dimensionality reduction.

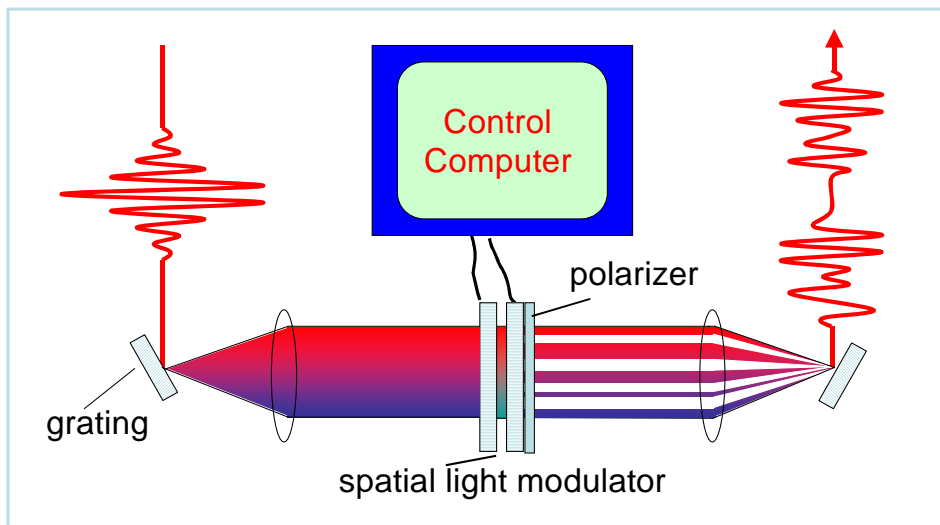


**Figure 4.** Pulse shaper to produce intense tailored pulses of  $\sim 50$  fs duration

## 2. Theory

### 2.1 Deterministic detection. Vector signal representation

In this section, we will consider how multi-dimensional analysis facilitates detection of a specific agent molecule in the presence of a background of interferences. As a simple proof-of-concept model for multiparameter adaptive data reshaping, we consider a situation when only two mass-spectral peaks are measured for a particular agent and an interferent (for the sake of simplicity we assume just one interferent is present). The signal from the chemical agent sought corresponds to a certain ratio of the intensities of these two peaks, while the signal from the interferent species corresponds to a different intensity ratio. We assume there is a macroscopically large number of molecules,  $N$ , in the ionization chamber, see Figure 5 for a schematic of the experimental arrangement. Some  $N_A$  of the molecules are agent molecules, other  $N_I$  are interferent molecules. As  $N_A + N_I = N$ , the probability to randomly pick an agent molecule is  $\nu = N_A/N$ , that is, the agent concentration, and the probability to pick an interferent molecule is  $1 - \nu$ . When a molecule is fragmented by a moderately strong laser pulse of a typical experiment, only one of its fragments is ionized.

Approaching the detection problem as a binary hypothesis testing, we take the null hypothesis to be  $\mathcal{H}_0: \nu = 0$ , the complete absence of agent and the alternative hypothesis to be  $\mathcal{H}_1: \nu > 0$ , the presence of agent in some unspecified concentration. To decide in favor of  $\mathcal{H}_1$  based on the measured values of the two measured mass-spectral peaks, these measurements should show the presence of some, however small, number of the agent molecules,  $n_A$ , out of total number  $n$  of the fragmented molecules. If the situation were purely deterministic, this demonstration would merely require simple algebra, as shown in the following paragraphs.

Both the agent and interferent signals can be visualized as signature vectors in the two-dimensional detection space whose coordinates are the peak heights,  $\mathbf{A} = (A_1, A_2)$  and  $\mathbf{I} = (I_1, I_2)$ , as shown in the lower right panel of Figure 5. In more general case, a multi-dimensional detection vector may be constructed from the fragmentation distribution for a particular molecule type. The components of the vector correspond to the two discrete mass values with the magnitudes of these components corresponding to the intensities of the mass peaks (number of ions in each of the two mass channels).

Note that for mass-spectroscopic peaks, the total number of molecules that have been ionized and fragmented equals the sum of the two peak heights. This sum of the heights defines the natural metric for the measurement of vectors (mathematically speaking, the detection space is a Banach space with  $L_1$  norm:  $\|\mathbf{V}\| = |V_1| + |V_2|$ ).

It is natural to normalize the signature vectors for agent and interferent by dividing out the number of molecules ionized to create these signature vectors (their  $L_1$  norms). So we assume the standard vectors  $\mathbf{A}$  and  $\mathbf{I}$  normalized to unity:

$$\begin{aligned} A_1 + A_2 &= 1; \\ I_1 + I_2 &= 1. \end{aligned} \tag{1}$$

Intuitively, it is clear that the agent and interferent will be discriminable in this experiment to the extent that these normalized signature vectors  $\mathbf{A}$  and  $\mathbf{I}$  define different directions. Notice that these vectors are well defined deterministic vectors in the limit of many molecules ionized to calculate them.

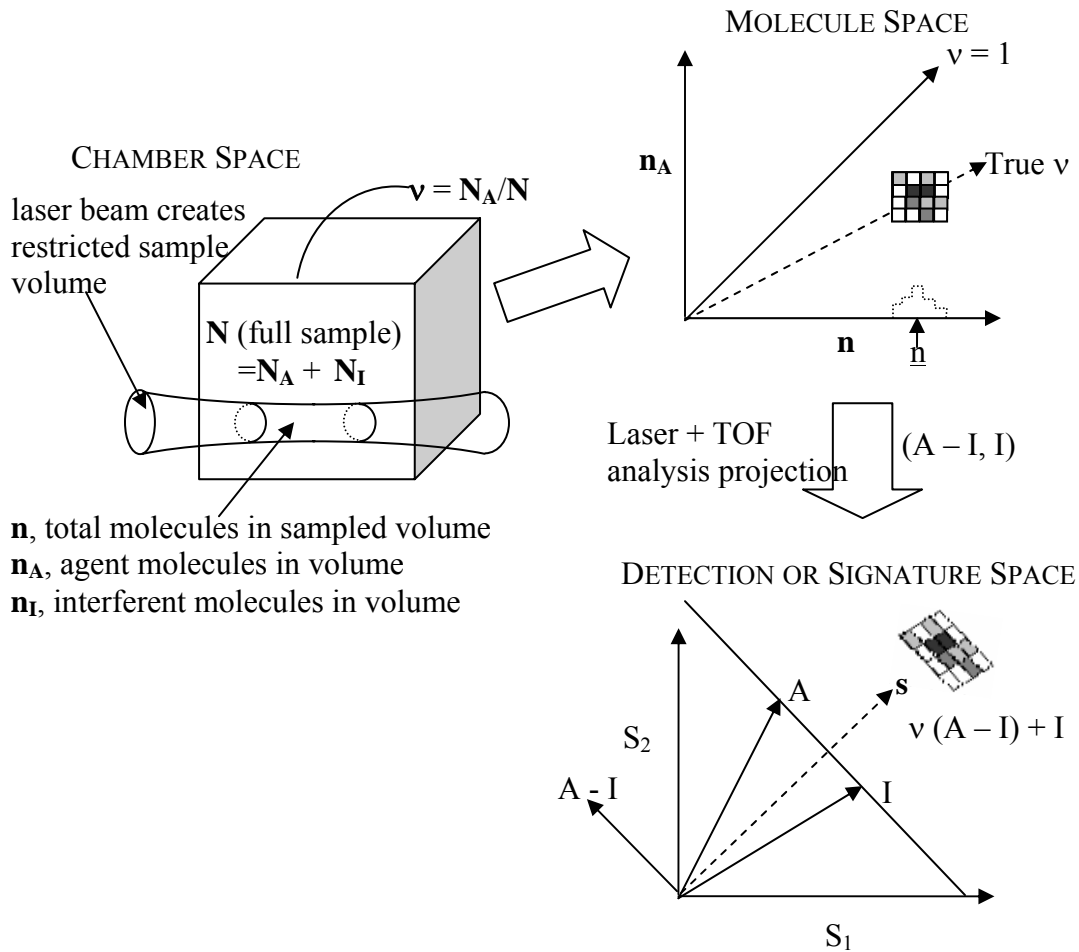


**Figure 5,** Depictions of the agent, interferent, and related detection signals in the chamber (physical) space, molecule space, and detection (signature) space.

Let us suppose that we have a mixture with a large number of both agent and interferent molecules and that various sources of noise and random error can be neglected. Then, the vector of the observed signal,  $\mathbf{s}$ , is comprised of the agent and the

interferent contributions:  $\mathbf{s} = n_A \mathbf{A} + n_I \mathbf{I}$ . The detection problem is to disentangle the contribution of the vector  $\mathbf{A}$ , and to determine whether its magnitude,  $n_A$ , is nonzero.

As all three vectors,  $\mathbf{s}$ ,  $\mathbf{A}$ , and  $\mathbf{I}$ , are known precisely, a direct disentanglement is straightforward: the system of equations,

$$\begin{aligned} n_A A_1 + n_I I_1 &= s_1 \\ n_A A_2 + n_I I_2 &= s_2 \end{aligned} \quad (2)$$

is easily solved to produce

$$\begin{pmatrix} n_A \\ n_I \end{pmatrix} = \frac{1}{A_1 I_2 - A_2 I_1} \begin{pmatrix} s_1 I_2 - s_2 I_1 \\ s_2 A_1 - s_1 A_2 \end{pmatrix}, \quad (3)$$

or, in terms of  $n_A$  and  $n$ ,

$$\begin{pmatrix} n_A \\ n \end{pmatrix} = \frac{1}{A_1 I_2 - A_2 I_1} \begin{pmatrix} s_1 I_2 - s_2 I_1 \\ s_2 (A_1 - I_1) - s_1 (A_2 - I_2) \end{pmatrix} = \hat{M} \begin{pmatrix} s_1 \\ s_2 \end{pmatrix} \quad (4)$$

Direct calculation of  $n_A$  from Eq. (4) solves the detection problem:  $n_A = (s_1 I_2 - s_2 I_1) / (A_1 I_2 - A_2 I_1) = 0$  corresponds to  $\mathcal{H}_0$ ;  $n_A > 0$  corresponds to  $\mathcal{H}_1$ . However, in this expression, the determinant becomes small if the vectors  $\mathbf{A}$  and  $\mathbf{I}$  are nearly collinear in the detection space, thus effecting extreme sensitivity of the predicted values  $n_A$  and  $n$  to possible errors in the data vector  $\mathbf{s}$  (a situation of so-called enhancing error propagation).

In fact, this is often just the case: random errors and fluctuations can be significant for complex molecules; as we will consider in detail in the next subsection. For now, let us get a sense of this by considering the opposite of the deterministic limit just considered. That is, how do the ionization signature vectors look like as the number of agent and/or interferent molecules becomes small? Here we encounter signature vectors which are intrinsically random, reflecting the uncertainty inherent in the quantum mechanics of molecular ionization and fragmentation.

To illustrate, suppose we are in the limiting case of exactly  $n=1$  molecule present in the ionizing volume. Suppose further it is known to be an agent molecule. In the deterministic limit of many molecules discussed above, we saw a mass peak signature vector proportional to the unit vector  $\mathbf{A} = (A_1, A_2)$  with constant of proportionality  $n_A$  the (large) number of agent molecules. However, with only one molecule of agent ionized we cannot expect to have fractional peaks. Instead we have an inherently random signature: We observe (1,0), corresponding to 1 count in mass-peak channel 1 and no counts in channel 2, with a probability  $A_1$ , and (0,1) with a probability  $A_2$ .

More generally, multiple molecules in the laser beam will ionize independently according to the above and sum to a net detected signature vector which is randomly distributed according to a multinomial distribution. We take up the details of this and other sources of random variation in the next subsection. For now, it suffices to say that the deterministic model and approach of this section is not relevant in many situations of interest in which the number of molecules of agent and/or analyte to be ionized is not large.

How will we deal with the detection problem in the presence of random fluctuations? The simple matrix inversion approach discussed in this section is no longer directly applicable. Instead, by developing and using simple probabilistic models of the errors we will upgrade the simple deterministic signal processing idea of equation (5) to create an optimal statistical detection procedure which allows one to

1. make the best call possible given the noisy data
2. provide performance bounds (probabilities of false alarm and missed detection)

These error bounds will show us that even with an optimal signal processing, the overall performance in detection is still limited by the possible proximity of the signature vectors **A** and **I** that would lead to error amplification in equation (5). To handle situations where this is the case, we go on to show that the signal and interferent vectors may be rotated in the detection Banach space to allow a more reliable detection call to be made.

## 2.2 Errors and fluctuations

In practice, the components  $s_1$  and  $s_2$  of the signature vector are obtained with some error; this error leads to corresponding error in the determined agent concentration. The causes for the uncertainties of the measured signal are of two kinds: (i) the uncertainties of associated with the ionized fragment production in the ionization chamber; and, (ii) the uncertainties associated with the detection of these fragments.

The detection uncertainties (the noise in the sensor detection system) are contributed by the thermal (dark current) noise in microchannel plates and the noise in the system electronics. This noise is usually insignificant; for instance the dark current noise is about 0.2 counts per second per square centimeter of the microchannel plate surface (used here) and can be safely neglected even at low signal levels of  $s_1, s_2 \sim 10$ .

The uncertainties of the ionized fragment production stem from several sources. Setting aside for now the quantum effects alluded to above, we must consider sampling fluctuations in the number and proportion of agent and interferent molecules caught in the laser focal region a small cylindrical volume,  $v_0$ , with characteristic diameter of 100  $\mu\text{m}$  and the length of 1 mm, where the laser pulse is focused to produce ionization). Fluctuations of the volume of the ionization region, and fluctuations of the ionization efficiency, both due to the fluctuations in the laser beam characteristics (the intensity and the pulse shape parameters) and are also potential contributors but in fact may be shown

to be insignificant in these experiments. The fluctuations of laser power have been measured to be less than 1%. If the ionization efficiency is saturated, which is typically the case at the laser intensities being used, it fluctuates even less than the laser power. Assuming the Gaussian transverse shape of the laser beam, we obtain the fluctuations of the cross-section area of the ionization volume due to the laser intensity fluctuations as  $\delta S = S_0 \delta I / I$ , where  $I$  is the maximum intensity at the center. Thus, the fluctuations of the ionization volume (and the number of molecules covered by this volume) are proportional to the relative fluctuation of the laser power:  $P(n - \bar{n}) = P(I - \bar{I})$  for the probability distributions.

Assuming we have a stable well defined laser ionization region, we can focus on the sampling variations. When a large population of molecules is in the chamber, what kind of sampling variations can we expect to see in the number and proportion of the two types that find themselves in this region when the laser is on? Fluctuations of the number of molecules,  $n$ , in the ionization volume can be estimated as follows. At typical operating pressure in the chamber  $\sim 10^{-6}$  Torr, the average number of molecules within the focal cylinder can be estimated as  $2.1 \times 10^5$ . Given  $\alpha \sim 1\%$  ionization efficiency, about 2000 ionized fragments are produced. This large average number justifies Gaussian statistics for the total number of ions and shows that fluctuations of this total number are relatively small ( $\sim 2\%$ ).

The combination of the two statistics leads to a relatively narrow distribution of the total number of the detected ions, that we can safely assume to have Gaussian shape:

$$P_0(n) = \frac{1}{\sqrt{2\pi\bar{n}}} \exp\left(-\frac{(n - \bar{n})^2}{2\bar{n}}\right) \quad (5)$$

where  $\bar{n} = \alpha N(v_0/V)$  is the average number of molecules ionized in the ionization volume.

As this analysis shows, the greatest degree of uncertainty, and, consequently, the efficiency of the binary hypothesis testing, is determined by the probability distributions of the agent and interferent ions as produced in the ionization volume. As we will presently see, these distributions are not independent.

### 2.3 Statistical distributions. Universal most powerful test

The probability to have exactly  $n_A$  agent ions and  $n_I = n - n_A$  interferent ions out of the total number of  $n$  ionized molecules is well approximated by the binomial distribution based on the agent concentration,  $\nu$ ,

$$P(n_A | n, \nu) = \binom{n}{n_A} \nu^{n_A} (1 - \nu)^{n - n_A} = \frac{n!}{n_A! (n - n_A)!} \nu^{n_A} (1 - \nu)^{n - n_A}. \quad (6)$$

The  $n_A$  agent ions and  $n_I$  interferent ions contribute to both  $s_1$  and  $s_2$  components of the measured vector  $s$ . These relative contributions are determined by the standard vectors  $\mathbf{A}$  and  $\mathbf{I}$ , respectively, and are also distributed binomially, so that for the  $s_1$ -component,

$$P(s_{1A} | n_A, A_1) = \binom{n_A}{s_{1A}} A_1^{s_{1A}} (1 - A_1)^{n_A - s_{1A}} = \frac{n_A!}{s_{1A}!(n_A - s_{1A})!} A_1^{s_{1A}} (1 - A_1)^{n_A - s_{1A}}; \quad (7)$$

$$P(s_{1I} | n_I, I_1) = \binom{n_I}{s_{1I}} I_1^{s_{1I}} (1 - I_1)^{n_I - s_{1I}} = \frac{n_I!}{s_{1I}!(n_I - s_{1I})!} I_1^{s_{1I}} (1 - I_1)^{n_I - s_{1I}}. \quad (8)$$

The binomial form of these distributions ensures the existence of a universal most powerful test. Indeed, we observe a total of  $s_1 + s_2 = n$  dissociations on a given trial and test the alternative hypothesis  $n_A > 0$  vs. the null hypothesis  $n_A = 0$ . The null hypothesis implies that all the  $n$  registered ions come from the interferent, that is, the measured values of  $s_1$  are expected to be binomially distributed according to Eq. (8) with  $s_{1I} = s_1$ ;  $n_A = n$ . Let us assume for certainty  $A_1 < I_1$ . This means that if there are some  $n_A > 0$  agent ions out of the  $n$  dissociations, one should on average obtain a smaller value of  $s_1$  than that provided by the distribution (8). Then, we employ the Neyman-Pearson most powerful test procedure [17] that provides the highest detection probability  $P_D$  given the false alarm probability  $P_{FA} = \alpha$ : we decide in favor of the alternative hypothesis if the likelihood ratio,

$$L(s_1) = \frac{P(s_1 | \mathcal{H}_1)}{P(s_1 | \mathcal{H}_0)} < \gamma, \quad (9)$$

where the parameter  $\gamma$  is chosen as

$$\sum_{s_1 \in \{L(s_1) > \gamma\}} P(s_1 | n, I_1) = \alpha. \quad (10)$$

Consider first a hypothetical extreme case:  $\mathcal{H}_1$  means all ions are of the agent. That is, we need to decide between  $n = n_I$  and  $n = n_A$ . Then,

$$L(s_1) = \frac{\binom{n}{s_1} A_1^{s_1} (1 - A_1)^{n - s_1}}{\binom{n}{s_1} I_1^{s_1} (1 - I_1)^{n - s_1}} = \left( \frac{1 - A_1}{1 - I_1} \right)^n \left( \frac{A_1 (1 - I_1)}{I_1 (1 - A_1)} \right)^{s_1} \quad (11)$$

Since this expression is monotonic in  $s_1$ , the condition of Eq. (10) means actually choosing the threshold value of  $s_1$ ,  $s_1 = s_{th}$ . For a given false alarm probability  $\alpha$ , we can set the  $s_1$ -threshold value of  $s_1 = s_{th}$  so that the left tail probability is  $\alpha$ :

$$P(s_1 \leq s_{th} | \mathcal{H}_0) = \sum_{k=0}^{s_{th}} P(k | n, \mathbf{I}) = \sum_{k=0}^{s_{th}} \binom{n}{k} I_1^k (1 - I_1)^{n - k} = \alpha \quad (12)$$

In a more realistic case of the alternative hypothesis representing some number of agent ions  $0 < n_A < n$ , the numerator of expression (9) assumes a more complicated form of

$\sum_{s_{1I}=0}^{s_1} P(s_{1I} | n - n_A, I_1) P(s_1 - s_{1I} | n_A, A_1)$  (see the discussion in the next section). As the value of  $n_A$  decreases from  $n_A = n$ , the peak of this numerator (as a function of  $s_1$ ) moves monotonically toward the peak of the denominator, thus devaluing the detection performance. However, the threshold value of  $s_1$  is still determined by Eq. (12) that does not contain the actual value of  $n_A$ . This means that the test under discussion is a universal most powerful test (UMP): for all possible decision criteria that have false alarm probability  $\alpha$ , the suggested threshold comparison  $s_1$  to  $s_{th}$  has the highest probability of correct detection (highest test power) regardless of the actual value of  $n_A$ .

## 2.4 Characteristic probabilities and the ROC curve

As stated in the previous section, the detection test performance, in terms of the detection probability and the false alarm probability, is primarily determined by the distributions of possible numbers of the agent and interferent ions in the detections volume, and by contributions of these two kinds of ions in the measured mass values of the fragments,  $s_1$  and  $s_2$ . To quantify the detection performance, we turn to a formal construction known as receiver operating characteristics (ROC) curve.

The detection procedure divides the set of all possible results of the measurements into two subsets, previously assigned as  $\mathcal{H}_0$  and  $\mathcal{H}_1$ . In a simple illustration case, the test can be performed on a one-dimensional signal. Then, all occurrences of a sensed signal exceeding a definite threshold value are assigned  $\mathcal{H}_1$  and all occurrences where the signal level is lower than threshold are assigned  $\mathcal{H}_0$ . When doing so, we intentionally miss that part of the true signal distribution that is below the threshold value, and include that part of the noise/interferent distribution that is above the threshold value. Let the signal and noise distributions be normalized to unity. Then, the area under the signal distribution curve above the threshold value is the probability for calling a true signal; the area under the noise distribution curve that resides above the threshold signal value gives the probability for calling a false positive signal.

There are four possible outcomes to consider when detecting a signal in the possible presence of noise and/or interferents. These outcomes are expressed in the four conditional probabilities:

- i.  $P(\mathcal{H}_1 | \mathcal{H}_1)$  – the probability of detection, that is, detection of agent when the agent is truly present;
- ii.  $P(\mathcal{H}_1 | \mathcal{H}_0)$  – the probability of a false alarm, i.e. the detection of agent when there is only noise or interferent;

- iii.  $P(\mathcal{H}_0 | \mathcal{H}_1)$  – the probability for a false negative detection, i.e., taking signal for noise/interference;
- iv.  $P(\mathcal{H}_0 | \mathcal{H}_0)$  – the probability of true negative outcome, that is, the absence of signal, so detected.

Among these probabilities, only two are independent, because the following obvious conditions hold:

$$\begin{aligned} P(\mathcal{H}_1 | \mathcal{H}_0) + P(\mathcal{H}_0 | \mathcal{H}_0) &= 1; \\ P(\mathcal{H}_1 | \mathcal{H}_1) + P(\mathcal{H}_0 | \mathcal{H}_1) &= 1. \end{aligned} \tag{2}$$

It is conventional to take  $P(\mathcal{H}_1 | \mathcal{H}_1)$  and  $P(\mathcal{H}_1 | \mathcal{H}_0)$  as the independent variables.

The point in the  $(P(\mathcal{H}_1 | \mathcal{H}_1), P(\mathcal{H}_1 | \mathcal{H}_0))$  plane that is given by a particular pair of probabilities is called the detector operating point corresponding to the chosen criterion (threshold value) [17]. A change in the threshold value will result in different values of  $P(\mathcal{H}_1 | \mathcal{H}_1)$  and  $P(\mathcal{H}_1 | \mathcal{H}_0)$  and in a different operating point in the  $(P(\mathcal{H}_1 | \mathcal{H}_1), P(\mathcal{H}_1 | \mathcal{H}_0))$  plane. The whole set of all the possible criteria generates a curve called the receiver operating characteristic curve (ROC). This curve is an important descriptor of the detector, because it specifies the false alarm rate as a function of detector sensitivity. By definition, the ROC is contained in the unit square near the origin in the positive quadrant of the  $(P(\mathcal{H}_1 | \mathcal{H}_1), P(\mathcal{H}_1 | \mathcal{H}_0))$  plane. As an illustration of ROC utility, Fig. 5 displays a series of ROC curves. The diagonal characteristic curve (actually, a straight line) corresponds to a coin flip with equal probability for true and false positive detection as a function of threshold value. The dashed line reveals a better characteristic curve with higher probability for true detection than a false positive event. The solid line displays a nearly perfect characteristic curve with the probability for a true positive detection,  $P(\mathcal{H}_1 | \mathcal{H}_1)$ , greatly exceeding the probability for false positive detection,  $P(\mathcal{H}_1 | \mathcal{H}_0)$ , for even the lowest threshold values. Numerically, the figure of merit is the area under the curve. The closer this area to unity, the better the detector operational characteristics.

To construct the ROC curve for the agent ion detection procedure determined by the probability distributions of Eqs. (6), (7), and (8), we first obtain the distribution of possible measured values of  $s_1$  and  $s_2$ . In the measured  $s_1$ , the probability to have contribution  $s_{1A}$  out of the  $n_A$  agent ions is given by Eq. (7) and the probability to have contribution  $s_{1I} = s_1 - s_{1A}$  out of the  $n - n_A$  interferent ions is given by Eq. (8). Summing over all the possible compositions of  $s_{1A}$  and  $s_{1I}$  having total of  $s_1$ , we obtain the probability to measure  $s_1$  as,

$$\begin{aligned}
P(s_1; n_A, n - n_A | \nu) &= \sum_{s_{1A} + s_{1I} = s_1} P(s_{1A}, n_A) P(s_{1I}, n - n_A) = \\
& n_A! (n - n_A)! (1 - A_1)^{n_A} I_1^{s_1} (1 - I_1)^{n - n_A - s_1} \sum_{s_{1A}=0}^{\min\{s_1, n_A\}} \frac{\left( \frac{A_1(1 - I_1)}{I_1(1 - A_1)} \right)^{s_{1A}}}{s_{1A}! (s_1 - s_{1A})! (n_A - s_{1A})! (n - n_A - s_1 + s_{1A})!}
\end{aligned} \tag{13}$$

When we sum this expression over all possible values of  $n_A$ , from zero to  $n$ , with the correspondent weights,  $P(n_A | n, \nu)$  of Eq. (6), and take into account that each time we measure  $s_1$  the rest  $n - s_1$  ions go to the  $s_2$  peak, we obtain the joint probability distribution function of the discrete random variables,  $s_1$  and  $s_2$ :

$$P(s_1, s_2) = (s_1 + s_2)! I_1^{s_1} (1 - I_1)^{s_2} (1 - \nu)^{s_1 + s_2} \sum_{n_A=0}^{s_1 + s_2} \left( \frac{\nu}{1 - \nu} \right)^{n_A} \left( \frac{1 - A_1}{1 - I_1} \right)^{n_A} \times \tag{14}$$

$$\frac{1}{n_A! (s_2 - n_A)!} {}_2F_1 \left( -n_A, -s_1, s_2 - n_A + 1, \frac{A_1(1 - I_1)}{I_1(1 - A_1)} \right)$$

where  ${}_2F_1(\dots)$  is the hypergeometric function [18].

Considering that the alternative hypothesis  $\mathcal{H}_1$  actually means the concentration of the agent molecules exceeding some harmful threshold value, it is natural and convenient to formulate the  $\mathcal{H}_1/\mathcal{H}_0$  set separation procedure in terms of the measured agent concentration rather than in measured value of  $s_1$  (or  $s_2$ ) peak (as symbolically depicted in Figure 5). For a given measured vector  $\mathbf{s} = (s_1, s_2)$ , the measured concentration of the agent is easily found from Eqs. (4) as:

$$\nu_m = \frac{s_1(1 - I_1) - s_2 I_1}{(A_1 - I_1)(s_1 + s_2)} \tag{15}$$

If a certain alarm-triggering threshold value of the measured intensity,  $\nu_{th}$ , is set, then all the points in the  $(s_1, s_2)$ -plane that lie below the straight line,

$$s_2 = \frac{1 - (I_1 + \nu_{th}(A_1 - I_1))}{I_1 + \nu_{th}(A_1 - I_1)} s_1 \tag{16}$$

correspond to  $\nu_m > \nu_{th}$  and thus trigger alarm. Thus, the probability of detection for a given  $\nu_{th}$  is

$$P(\mathcal{H}_1 | \mathcal{H}_1) = \int_{\nu_i}^1 d\nu \sum_{s_1=0}^{\infty} \sum_{s_2=0}^{\infty} P_0(s_1 + s_2) P(s_1, s_2 | \nu) \Theta \left( \frac{1 - (I_1 + \nu_{th}(A_1 - I_1))}{I_1 + \nu_{th}(A_1 - I_1)} s_1 - s_2 \right) \tag{17}$$

where  $\Theta(x)$  is the Heaviside function; the probability of a false alarm is

$$P(\mathcal{H}_1 | \mathcal{H}_0) = \int_0^{\nu_t} d\nu \sum_{s_1=0}^{\infty} \sum_{s_2=0}^{\infty} P_0(s_1 + s_2) P(s_1, s_2 | \nu) \Theta \left( \frac{1 - (I_1 + \nu_{th}(A_1 - I_1))}{I_1 + \nu_{th}(A_1 - I_1)} s_1 - s_2 \right) \quad (18)$$

The parametric plot  $(P(\mathcal{H}_1 | \mathcal{H}_1), P(\mathcal{H}_1 | \mathcal{H}_0))$  as functions of  $\nu_{th}$  gives the ROC curve. As seen in Eqs. (5), (14), (17), and (18), this curve depends on several factors. First, there is obvious dependence on the total number of registered ions,  $\bar{n}$ , and on the true agent concentration,  $\nu_t$ . Increasing  $\bar{n}$  or  $\nu_t$  naturally leads to more confident detection. More interesting is the fact that there is a dependence on the directions of the standard vectors  $\mathbf{A}$  and  $\mathbf{I}$  in the detection plane, as expressed by the parameters  $A_1$  and  $I_1$ . In particular,  $2|A_1 - I_1|$  gives the distance between the two vectors in the  $L_1$  metric. In the next section, we illustrate this dependence by numerical example and show that distance-increasing modification of the standard vectors can indeed substantially improve the detection performance in terms of ROC characteristics.

## 2.5 Numerical analysis of ROC modification

To illustrate the claim that disentangling the vectors  $\mathbf{A}$  and  $\mathbf{I}$  dramatically improves the detector capabilities, we simulate the receiver operating curve for agent/interferent discrimination in two cases that differ by the extent of how well the interferent mimics the agent. For the sake of illustrative simplicity, we assume the  $P_0(n)$  distribution to be very narrow so the number of ions,  $\bar{n}$ , is essentially constant. We also assume that we only need to discriminate between only two values of the agent concentration,  $\nu = \nu_t$  and  $\nu = 0$ . With these simplifications, formulas (17) and (18) reduce to

$$P(\mathcal{H}_1 | \mathcal{H}_1) = \sum_{s_1=0}^{\bar{n}} P(s_1, \bar{n} - s_1 | \nu) \Theta(s_1 - (I_1 + \nu_{th}(A_1 - I_1))\bar{n}) \quad (19)$$

$$P(\mathcal{H}_1 | \mathcal{H}_0) = \sum_{s_1=0}^{\bar{n}} P(s_1, \bar{n} - s_1 | 0) \Theta(s_1 - (I_1 + \nu_{th}(A_1 - I_1))\bar{n})$$

We consider two cases that refer to the experimental situation presented later in Section 3.

**Case I:** We assume the agent and the interferent standard vectors to be  $\mathbf{A} = (0.5, 0.5)$  and  $\mathbf{I} = (0.2, 0.8)$ , respectively. We take the actual agent concentration  $\nu_t = 0.5$  and the number of fragmented ions,  $\bar{n} = 15$ . The receiver operating curve for this situation is shown in Fig. 6a; its apparently discretized shape is due to relatively small number of the detected ions. As can be seen, the ratio of the areas into which the curve cuts the upper triangle is about  $2/3$ , which indicates rather poor detection performance.

**Case II:** Now, we assume the agent standard vector to have being rotated to  $A = (0.7, 0.3)$  while the interferent vector is the same as in Case I,  $I = (0.2, 0.8)$ . This modest disentangling rotation results in considerable improvement in the receiver operating curve, as shown in Fig 6b. (The actual agent concentration and the number of fragmented ions are the same as in Case I,  $\nu_i = 0.5$  and  $\bar{n} = 15$ , respectively.) It is only 1/6 of the total area of the upper triangle that lies above the curve. As will be seen in Section 3, this degree of vector rotation can be easily achieved by changing the shape of the probing signal in the laser-based mass spectrometry. Note also that we actually consider the worst-case scenario of low-signal detection; an increase in the total number of detected ions will considerably sharpen the probability distributions and make the effect of disentangling vector rotation much more pronounced. Thus, we have shown that adaptive modification of the probing signal can improve the detection performance in the most difficult case of low signal-to-noise ratio.

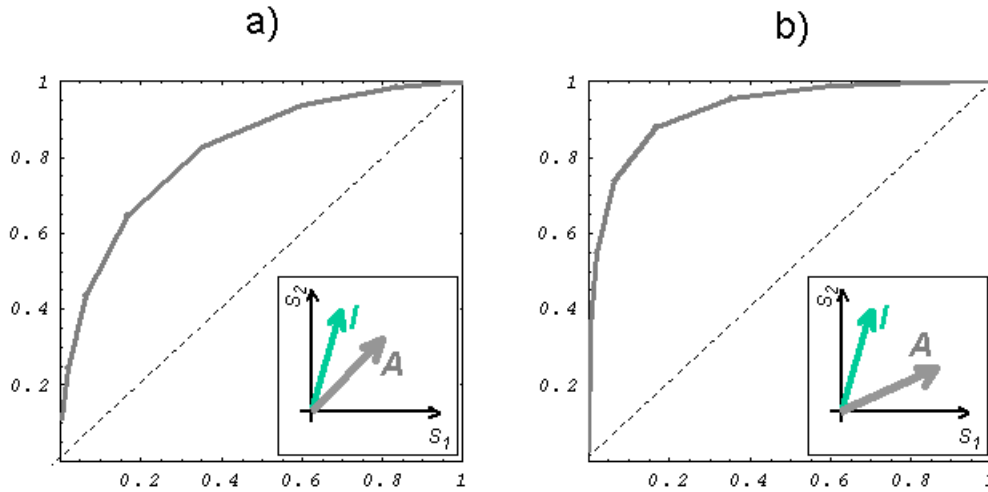


**Fig. 6.** ROC curves in cases of **a**, an interferent that mimics the agent peak intensity ratio well; and **b**, the agent signature that has been manipulated to be masked by the interferent peak intensity ratio less well. The marked improvement in the detection performance is due to disentangling rotation of the standard vectors  $A$  and  $I$ , shown in the inserts.

### 3. Examples of vector modification by adaptively shaped pulses

As a specific implementation of adaptive probe manipulation that produces signal vector rotation, we consider the detection of complex polyatomic molecules using time-of-flight mass spectrometry. In this example the molecule is ionized and fragmented by a strong-field, ultrafast laser pulse.

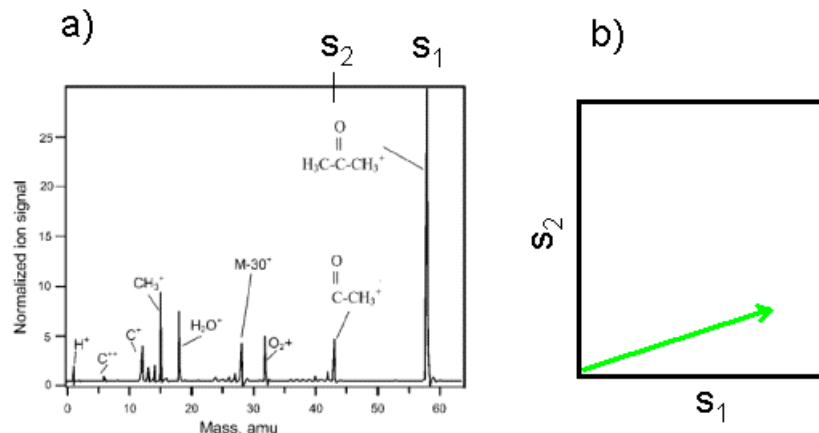


**Fig. 7.** A fragmentation pattern of acetone subjected to an intense transform-limited laser pulse [4].

We first demonstrate the feasibility of using laser pulse shaping to achieve maximum rotation of an agent-of-interest vector. Here we implement the adaptive vector rotation method to the fragmentation pattern of a typical polyatomic molecule, acetone,  $(\text{CH}_3)_2\text{CO}$ , as an initial example. Figure 7a displays the mass spectrum resulting from the interaction of acetone vapor with a transform-limited (i.e. Gaussian-shaped) pulse of duration 80 fs and intensity  $10^{13} \text{ W}\cdot\text{cm}^{-2}$ . The laser pulse had an intensity of 1 mJ and was focused to a  $100 \mu\text{m}$  diameter in the extraction region of the time-of-flight mass spectrometer shown in Figure 2. The laser intensity reached in this focused, ultrafast pulse is sufficient to ionize the molecule through both multiphoton processes and through tunnel ionization. Furthermore, the intensity is sufficient to dissociate the molecule through a variety of mechanisms. The various ionization/dissociation processes lead to the plethora of fragmentation peaks observed in the mass spectrum in addition to the parent molecular ion detected at 58 atomic mass units.

Figure 7 displays a number of mass-spectral peaks corresponding to various photoreaction channels. We concentrate on two peaks: (i)  $(m/e) = 58$  amu corresponding to simple removal of an electron from the molecule to produce the intact acetone radical cation; (ii)  $(m/e) = 43$  amu corresponding to cleavage of one methyl group to produce the  $\text{CH}_3\text{CO}$  (methyl carbonyl) ion and  $\text{CH}_3$  (methyl) molecule/ion. In the mass spectrum of Fig. 8a, the ratio of these two peaks,  $\text{CH}_3/\text{CH}_3\text{CO}$ , is about 0.15. Based on the intensity of these two peaks, the mass spectrum can be transformed into a two-dimensional parameter space as shown in Figure 8b. In doing so, we normalize the peak heights by the total fraction of molecules fragmented into either the parent ion or methyl carbonyl ion, and discard the information carried by all the other peaks in the mass-spectrum. To manipulate the two-dimensional representative vector, we search the potential laser pulse

shapes using an evolutionary learning algorithm. As a first example, the vector was rotated to project almost entirely along the ordinate axis (producing mainly parent molecular ion). In this case, the ratio  $(H_2/H_1) \sim 0.02$  was achieved. The corresponding mass spectrum and the representing vector are shown in Figure 8a and c. As a second example, maximum rotation of the vector toward the vertical axis was specified by maximizing the methyl carbonyl to parent ion yield ratio  $((H_2/H_1) \sim 0.75)$ . The corresponding mass spectrum and the representing vector are shown in Figure 8b and d. This effective rotation was achieved by the fifth generation of the closed-loop genetic algorithm. This occurred in a reasonable amount of laboratory time ( $\sim 5$  min). This experiment clearly demonstrates that adaptive pulse shaping is capable of dramatic alteration of the information content in a mass spectrum, thus paving the way to the desired signal preprocessing.

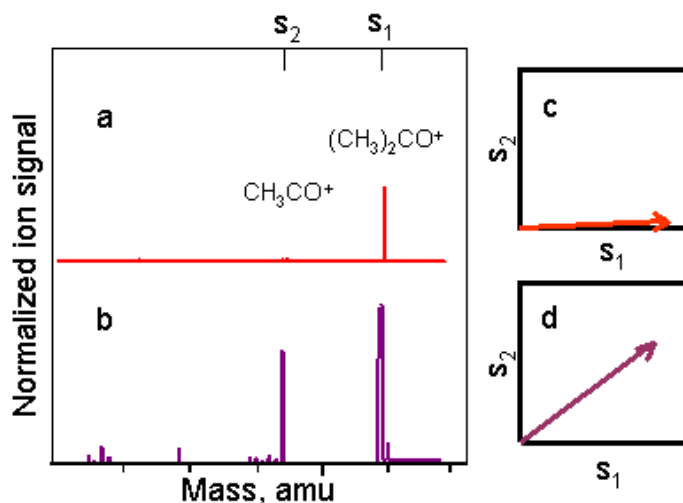


**Figure 8.** Rotation of the two-dimensional vector representing the acetone fragmentation pattern by manipulating the amplitudes of the parent ion and methyl carbonyl peaks. **a**, the mass spectrum resulting from a shaped laser pulse maximizing the parent molecular ion; **b**, the mass spectrum resulting from a shaped pulse maximizing the methyl carbonyl fragment; **c**, the two-dimensional representation of the mass spectrum shown in a; **d**, the two-dimensional representation of the mass spectrum shown in b. The rotation was achieved by adaptive laser pulse shaping.

A typical polyatomic molecule allows manipulation of a given peak ratio on the order of a factor of two to ten with a strong field shaped laser pulse. Assuming this typical range of manipulation for both the agent and interferent in the discrimination setting, and having in hand a practically infinite number of accessible pulse shapes, one anticipates about the same range of the vector separation between agent and interferent. There is one major practical difficulty, however, in finding the pulse shape that realizes the desired optimal separation. This is the problem of finding a pulse shape to maximize

discrimination for molecules with overlapping fragmentation distributions. The question concerns how one determines the pulse shape in practice that will maximize discrimination given the fact that the fragments of interest overlap. To this end, several strategies can be envisioned. First, for a fast, though non-optimal solution one can draw on a pool of random, but characterized, pulse shapes associated with rotations of each of the two molecule's vectors measured individually, that is, with only one of the two species present in the chamber: the pulse producing most separated vectors will be the best choice on the given subset. This requires a set of library pulses, and the optimal pulse may not be contained therein. Second, in a more elaborate experimental approach, adaptive pulse shaping can be achieved by using simultaneous monitoring of the fragmentation patterns of the agent of interest and the interferent in separate chambers. This solution has the opportunity to optimize the vector rotation for a given pair of molecules, but requires  $n$  analysis chambers to determine the pulse shape that maximally discriminates  $n$  overlapping features. We present here a third option for directly determining the optimal pulse to discriminate agent and interferent that requires only one analysis chamber for  $n$  features. The method is based on isotopic labeling to separate agent and interferent signals in the mass spectrometer.

As a second demonstration of the concept of vector rotation we investigate whether the detection vectors for two molecules having a two overlapping mass spectral features can be independently rotated to vary the fragmentation distribution independently for each molecule. In this experiment we adaptively manipulate the mass spectra for a mixture of the molecules acetone and trifluoroacetone. When these molecules are ionized and fragmented by a strong field laser pulse, each has dissociation channels that produce the  $\text{CH}_3^+$  and  $\text{CH}_3\text{CO}^+$  fragments. For the (normally) hydrogenated molecules, the mass spectral peaks for these channels perfectly overlap, and thus acetone would be an interferent for identifying trifluoroacetone, and vice versa. When the hydrogen isotopes of the molecules are employed, the task of finding pulse shapes that manipulate the fragment distributions independently is a difficult task. Here we present a simple method based on isotopic labeling to simultaneously optimize the discrimination pulse for a mixture of the two molecules. In this investigation we employ deuterated acetone ( $\text{d}_6$ -acetone), but deuterated trifluoroacetone would work just as well. Full deuteration of acetone translates the methyl and methoxy peaks by three mass units in the mass spectrum. This allows a simple contrast mechanism for mass spectral identification and the molecules can be independently addressed with the same laser pulse in a mixture in a single analysis experiment.

The isotopic labelling method for mass spectral discrimination assumes that deuteration, for example, does not significantly alter the control mechanism in comparison to the hydrogenated molecule. That is, we assume that the control pulse that dissociates deuterated acetone in a given fragment distribution will also dissociate normal acetone in a similar fashion. This is a reasonable assumption in the limit of strong laser fields because the coupling between the laser field and the molecule occurs through the electrons rather than through vibrational modes of the molecule.

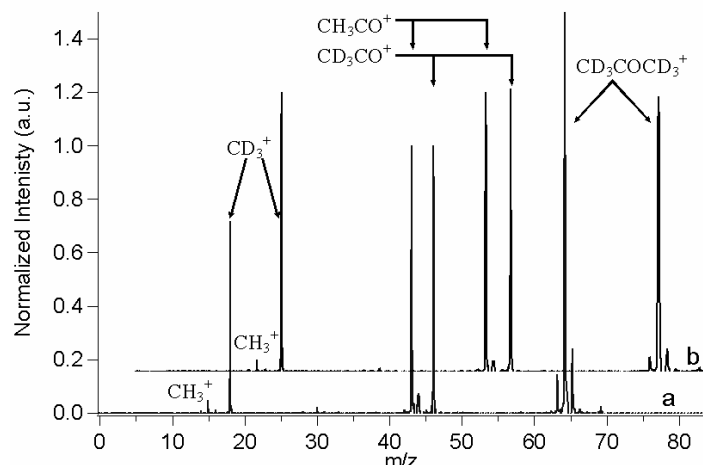


**Figure 9**, the strong field mass spectra for the mixture of deuterated acetone and trifluoroacetone. The spectrum resulting from a 60 fs pulse is shown in **a** and the optimized spectrum is shown in **b**.

The mass spectra for the  $d_6$ -acetone and the trifluoroacetone are shown in Figure 9. The methyl ( $\text{CH}_3^+$ ) and methoxy ( $\text{CH}_3\text{CO}^+$ ) features are located at 15 and 41 amu, respectively for trifluoroacetone. The deuterated methyl ( $\text{CD}_3^+$ ) and methoxy ( $\text{CD}_3\text{CO}^+$ ) features are detected at 18 and 44 amu, respectively, for  $d_6$ -acetone. The mass spectrum for the acetone/trifluoroacetone mixture for the case of the average of the initial pulse shapes is shown in Figure 9a. This corresponds to detection vectors for acetone and trifluoroacetone, as shown by the solid vectors in Figure 10. The control objective was set to rotate the detection vectors as far apart as possible for the two molecules by using a fitness criterion as follows:

$$f = \left| \tan^{-1} \left( \frac{M_{2I}}{M_{1I}} \right) - \tan^{-1} \left( \frac{M_{2A}}{M_{1A}} \right) \right| \quad (20)$$

The optimized mass spectrum is shown in Figure 10b. This corresponds to a rotation of the detection vectors, as shown by the dotted vectors in Figure 10. In this case the majority of the rotation occurred by increasing the fractional yield of the methyl species in acetone while almost no change in the trifluoroacetone dissociation pattern occurred.

Without the deuteration of the acetone, the measured signal vector would be the sum of the amplitudes for the methyl and methoxy for both the acetone and the trifluoroacetone molecules. In this experiment reported here we demonstrate that a pulse shape can be optimized to maximize the angle between the detection vectors of the two molecules and thus change the overall direction of the signal. Summing the vectors reveals that the detection vector would be rotated by approximately 10 degrees with the optimized pulse in comparison to the 65 fs pulse.

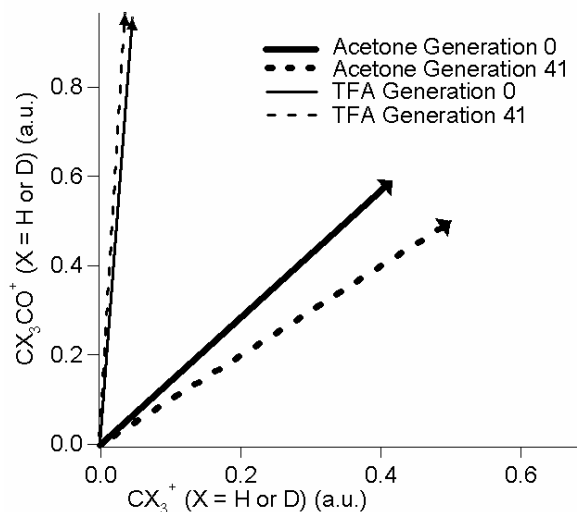


**Figure 10.** A two-dimensional Banach space plot of the signal/interferent vectors for trifluoroacetone and fully deuterated acetone. The solid lines correspond to the initial detection vectors for the molecules and the dotted line vectors correspond to the detection vectors after optimization of the rotation.

#### 4. Conclusions and prospects

We have developed theoretically, and demonstrated experimentally, a proactive detection approach to manipulate the probing signal to channel the outcome of the probe-target interaction into the most statistically significant dimensions of the sensing data search space. The payoff is a significant improvement in the detection performance on a background of noise and signal-mimicking interferences. This detection scheme possesses inherent adaptivity to interference, because it is capable of opening extra dimensions to discriminate between the agent and the interfering signal even in the high noise situation ( $N_a \ll N_i$ ). The proposed approach can be easily modified to adjust to experiments requiring either detection to recognize the presence of an agent in small amount on the substantial background or classification to distinguish between two or more different agents. Furthermore, in laboratory detection systems there is a balance between the speed vs. sensitivity and speed vs. universality. Accordingly, a set of optimal protocols can be developed to suit various strategies, based on a library of discriminating signals.

#### 5. Acknowledgements

The authors wish to thank the generous support of the DoD MURI program as administered through the Army Office of Scientific Research, the National Science Foundation, and DARPA.

## References

- [1] R. Bellman, "Adaptive Control Processes: A Guided Tour," Princeton University Press, 1961.
- [2] D. W. Scott, *Multivariate Density Estimation*. New York: Wiley, 1992.
- [3] C. E. Priebe, D. J. Marchette, and D. M. Healy, "Integrated sensing and processing decision trees," *Ieee Transactions on Pattern Analysis and Machine Intelligence*, vol. 26, pp. 699-708, 2004.
- [4] R. J. Levis and H. A. Rabitz, "Closing the loop on bond selective chemistry using tailored strong field laser pulses," *Journal of Physical Chemistry A*, vol. 106, pp. 6427-6444, 2002.
- [5] R. S. Judson and H. Rabitz, "Teaching Lasers to Control Molecules," *Physical Review Letters*, vol. 68, pp. 1500-1503, 1992.
- [6] M. M. Wefers and K. A. Nelson, "Ultrafast Optical Wave-Forms," *Science*, vol. 262, pp. 1381-1382, 1993.
- [7] D. Meshulach, D. Yelin, and Y. Silberberg, "Adaptive real-time femtosecond pulse shaping," *Journal of the Optical Society of America B-Optical Physics*, vol. 15, pp. 1615-1619, 1998.
- [8] A. M. Weiner, "Femtosecond pulse shaping using spatial light modulators," *Review of Scientific Instruments*, vol. 71, pp. 1929-1960, 2000.
- [9] T. Brixner, A. Oehrlin, M. Strehle, and G. Gerber, "Feedback-controlled femtosecond pulse shaping," *Applied Physics B-Lasers and Optics*, vol. 70, pp. S119-S124, 2000.
- [10] R. J. Levis, G. M. Menkir, and H. Rabitz, "Selective bond dissociation and rearrangement with optimally tailored, strong-field laser pulses," *Science*, vol. 292, pp. 709-713, 2001.
- [11] N. P. Moore, G. M. Menkir, A. N. Markevitch, P. Graham, and R. J. Levis, "The Mechanisms of Strong-Field Control of Chemical Reactivity Using Tailored Laser Pulses," in *Laser Control and Manipulation of Molecules*, R. J. Gordon, Ed.: ACS Symposium Series in Chemistry, 2001.
- [12] D. Strickland and G. Mourou, "Compression of amplified chirped optical pulses," *Optics Communications*, vol. 56, pp. 219-221, 1985.
- [13] A. M. Weiner, D. E. Leaird, J. S. Patel, and J. R. Wullert, "Programmable Shaping of Femtosecond Optical Pulses by Use of 128-Element Liquid-Crystal Phase Modulator," *IEEE Journal of Quantum Electronics*, vol. 28, pp. 908-920, 1992.
- [14] A. M. Weiner, "Femtosecond Optical Pulse Shaping and Processing," *Progress in Quantum Electronics*, vol. 19, pp. 161-237, 1995.
- [15] M. M. Wefers and K. A. Nelson, "Programmable Phase and Amplitude Femtosecond Pulse Shaping," *Optics Letters*, vol. 18, pp. 2032-2034, 1993.
- [16] M. J. DeWitt and R. J. Levis, "Observing the transition from a multiphoton-dominated to a field-mediated ionization process for polyatomic molecules in intense laser fields," *Physical Review Letters*, vol. 81, pp. 5101-5104, 1998.
- [17] S. M. Kay, *Fundamentals of Statistical Signal Processing, vol. II: Detection Theory*. Upper Saddle River, NJ: Prentice Hall, 1998.

- [18] M. Abramowitz and I. A. Stegun, "Handbook of mathematical functions with formulas, graphs, and mathematical tables." Washington, D.C.: United States Department of Commerce : U.S. Government Printing Office, 1972.